DOI: 10.24425/ame.2025.154743

2025, Vol. 72, No. 3, pp. 545-561



Free flexural axisymmetric vibration of a clamped circular sandwich plate with a functionally graded core

Received 28 April 2025, Revised 25 July 2025, Accepted 28 July 2025, Published online 11 August 2025

Keywords: composite plate, shear deformation theory, five-layered structures

This study presents an analytical model of a clamped circular sandwich plate with a functionally graded core, developed within the framework of an individual nonlinear shear deformation theory. The mathematical formulation is an original contribution, providing a unified representation of various structural configurations – including three-layer-like, five-layer-like, homogeneous single-layer, and intermediate forms – through a single continuous function. The variation of Young's modulus across the core is controlled by three parameters, enabling flexible modeling of material gradation.

The governing equations are derived using Hamilton's principle and are solved analytically through an approximate solution method. The proposed model allows investigation of the effects of material property variation and the core-to-plate thickness ratio on the fundamental natural frequency, as well as on the shear effect coefficient and plate mass, yielding general conclusions supported by a coherent theoretical framework.

1. Introduction

Composite constructions are undergoing rapid development due to their high strength-to-weight ratios and adaptability in engineering applications. Among the numerous challenges in their analysis and design, the study of free vibrations plays a crucial role. Meiche et al. [1] introduced a novel hyperbolic shear deformation theory for buckling and free vibration analysis of thick functionally graded sandwich plates. This approach yields only four governing equations and unknowns – fewer than the five required in classical shear deformation theories such as those

²Łukasiewicz Research Network – Poznan Institute of Technology, Poznan, Poland



[⊠] Ewa MAGNUCKA-BLANDZI, e-mail: ewa.magnucka-blandzi@put.poznan.pl

¹Poznan University of Technology, Institute of Mathematics, Poznan, Poland

of Mindlin and Reissner. Importantly, it does not require a shear correction factor while maintaining high accuracy, comparable to that of higherorder models. Thai and Vo [2] proposed a sinusoidal shear deformation theory for functionally graded plates that addresses bending, buckling, and vibration problems. Their theory incorporates a sinusoidal distribution of transverse shear stress and satisfies traction-free boundary conditions without requiring correction factors, using just four unknowns. Closed-form solutions for simply supported plates demonstrate their efficiency and precision. Mahi et al. [3] developed another hyperbolic shear deformation theory applicable to various plate types – including isotropic, functionally graded, laminated, and sandwich structures. This model, which introduces five degrees of freedom, ensures parabolic shear strain distribution and satisfies zero-traction boundary conditions without correction factors. Using Hamilton's principle and the Ritz method, the study provides accurate analytical solutions for deflections, stresses, and vibration frequencies. Chen et al. [4] analyzed free and forced vibrations of functionally graded porous beams with spatially varying porosity and material properties. Their approach integrates Timoshenko beam theory with Lagrange's equations, Ritz trial functions, and the Newmark- β method to explore both symmetric and asymmetric porosity effects. The study reveals how these distributions affect dynamic performance under different loading conditions. Singh and Singh [5] introduced two advanced shear deformation models – Trigonometric Deformation Theory (TDT) and Trigonometric-Hyperbolic Deformation Theory (THDT) – for laminated and 3D braided composite plates. These theories incorporate nonlinear shear strain distributions that meet surface traction-free conditions. Numerical results show superior accuracy in predicting vibration and buckling behavior, with sensitivity to parameters like fiber volume fraction and braiding angle. Zhai et al. [6] focused on five-layered sandwich plates with double viscoelastic cores, analyzing their free vibration behavior using first-order shear deformation theory. The governing equations derived through Hamilton's principle were solved via the Navier method, providing new benchmark data on frequency and damping characteristics. Żur [7] investigated free vibrations of functionally graded circular plates supported by concentric rings using classical plate theory. Employing the quasi-Green's function method, the study evaluates how boundary conditions, volume fraction index, and support geometry influence natural frequencies, offering reference values for model validation. Birman and Kardomateas [8] reviewed contemporary developments in sandwich structures, addressing theoretical progress, core innovations, and application challenges. Their work emphasizes the role of damage mechanisms and environmental effects in shaping future research across sectors such as aerospace, civil engineering, electronics, and biomedicine. Magnucki et al. [9] examined a rectangular plate with symmetrical through-thickness variation in mechanical properties, applying a nonlinear deformation hypothesis. By deriving motion equations via Hamilton's principle and solving them analytically, they determined critical loads and natural frequencies. Their findings were further validated through finite element modeling using ABAOUS. Zur et

al. [10] investigated the free vibration and buckling responses of functionally graded nanoplates incorporating magnetoelectro-elastic coupling, employing a nonlocal modified sinusoidal shear deformation theory. The motion equations, derived via Hamilton's principle, include contributions from electric and magnetic fields. Analytical solutions for simply supported plates were validated against existing results, and a parametric study revealed the influence of various factors on the nanoplate's mechanical behavior. These outcomes provide benchmark data for validating analytical and numerical methods in nanoelectromechanical system (NEMS) design. Roshanbakhsh et al. [11] introduced an analytical approach based on displacement potential functions to solve the three-dimensional free vibration problem of functionally graded circular plates with surface boundary conditions. Material properties vary according to exponential and power laws. The method decouples the governing equations into linear partial differential equations, which are solved independently. Solutions are presented for isotropic FG materials under axisymmetric vibration and in-plane shear modes, demonstrating high accuracy and agreement with previous analytical studies and ABAQUS simulations. Magnucki [12] addressed the axisymmetric flexural vibrations of circular plates with clamped edges and symmetric through-thickness property variation, supported on elastic foundations. A shear deformation model was used to derive the motion equations, and the fundamental natural frequency was obtained analytically. Magnucki et al. [13] studied a simply supported circular plate with thickness-wise variations transitioning between single-layer and three-layer configurations. A unified mathematical formulation for axisymmetric bending and buckling – including intermediate structural states – was developed, accounting for shear effects. The governing equations were solved analytically. Sah and Ghosh [14] explored free vibration and buckling of multidirectional porous FGM sandwich plates with continuously varying material properties along the longitudinal and transverse directions. Voigt's micromechanical model and sinusoidal shear deformation theory were used to derive equilibrium equations. An analytical solution using Navier's technique was obtained, and the influence of porosity distribution, volume fraction indices, layer thickness, and geometric parameters on natural frequencies and buckling loads was evaluated. Wei and Oing [15] applied modified couple stress theory (MCST) to study axisymmetric bending, buckling, and free vibration of circular and annular microplates made from bi-directional functionally graded (BiFG) materials. Hamilton's principle was employed to derive the governing equations and boundary conditions, discretized using the generalized differential quadrature method. Numerical results illustrated the effects of material and geometric parameters on mechanical responses under various edge constraints. Magnucki [16] investigated three-point bending of simply supported beams, including homogeneous, sandwich, and depth-graded structures with bisymmetrical cross-sections. Analytical models were developed incorporating the Zhuravsky shear stress formula, and using the principle of stationary total potential energy, differential equilibrium equations were solved. Deformations and maximum deflections were analytically determined and visualized. In [17], Mag-

nucki and Magnucka-Blandzi modeled free axisymmetric flexural vibrations of a three-layer sandwich circular plate with a graded core and constant facings. A nonlinear shear deformation theory was developed, and cases of simply supported and clamped edges were analyzed using Hamilton's principle. The resulting motion equations yielded fundamental natural frequencies. Magnucki et al. [18] examined an asymmetrical sandwich beam with a functionally graded core under three distinct boundary condition variants. Employing Hamilton's principle, they developed an analytical model leading to two differential equations of motion, which were solved to determine critical loads and fundamental natural frequencies for each support case. Detailed calculations for exemplary beam configurations were performed and compared with results from finite element analysis. In a subsequent study, Magnucki et al. [19] investigated a thin-walled rectangular sandwich plate featuring an individually functionally graded core. Utilizing a nonlinear shear deformation theory based on the concept of a straight normal, a reduced system of equilibrium equations was derived and solved analytically to determine the critical load. Additional analytical analyses were conducted for selected plates, complemented by a corresponding FEM-based numerical model. Bardella [20] provided analytical solutions for the stress field in straight sandwich beams with identical face sheets, considering linear elastic flexure influenced by zigzag warping and Timoshenko's kinematics. An equilibrium equation from Cauchy continuum mechanics was employed to recover the through-thickness normal stress component. The accuracy of these estimates was demonstrated across a range of stiffness ratios and boundary conditions. By comparing with detailed FEM simulations, the study highlighted the significance of tensile stress at the core–face interface in cantilever sandwich beams under uniform loads, underscoring its importance in delamination analyses and reliable sandwich panel design. This study concerns a clamped circular sandwich plate with radius R and total thickness h, featuring an individually functionally graded core (see Fig. 1) between facings with constant mechanical properties. The work is a continuation of previous analyses on circular plates reported in [12, 13, 17], and an improvement of their analytical models. The main goal of the work is to develop an analytical model of this plate that incorporates shear deformation effects, and to determine the fundamental natural frequencies of selected plate configurations.

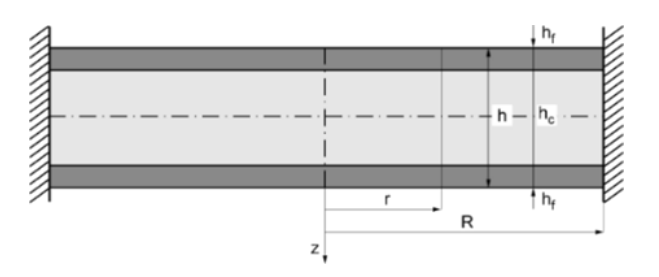


Fig. 1. Scheme of the clamped circular sandwich plate



Based on Hamilton's principle, two differential equations of motion for the clamped circular plate are derived and then approximately solved by assuming specific forms for the unknown functions that satisfy the boundary conditions of the clamped plate. Finally, the fundamental natural frequency is obtained.

The total thickness of the plate is expressed as the sum of the following layers

$$h = 2h_f + h_c \,, \tag{1}$$

where: h_f – thickness of each facing, h_c – thickness of the core.

2. The analytical model of the circular sandwich plate

Fig. 2 illustrates the distribution of Young's modulus across the plate's thickness.

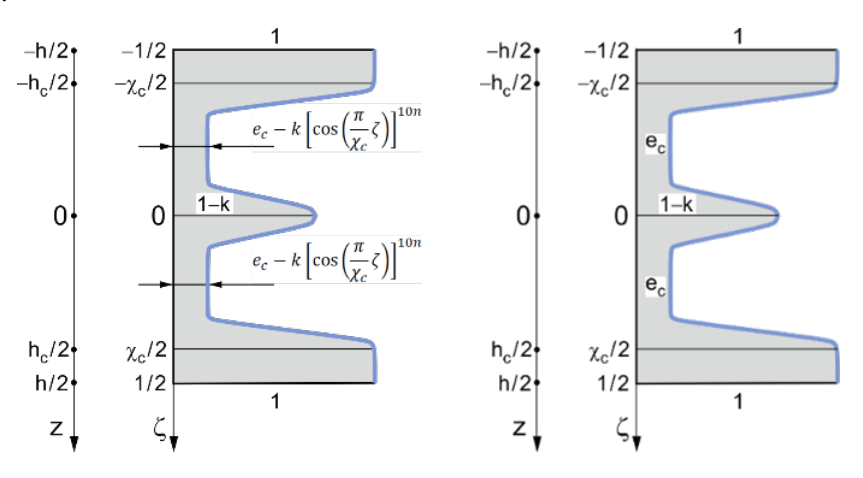


Fig. 2. Variation of Young's modulus along the plate thickness (left) and simplified representation for larger values of n (right)

The Young's modulus is defined based on the formulation proposed in [19]. In the upper $(-1/2 \le \zeta \le -\chi_c/2)$ and lower facing $(\chi_c/2 \le \zeta \le 1/2)$, it is constant and equal to E_f , whereas in the core $(-\chi_c/2 \le \zeta \le \chi_c/2)$, it varies according to the following expression:

$$E_c(\zeta) = E_f f_e(\zeta),\tag{2}$$

where the dimensionless function

$$f_e(\zeta) = e_c + (1 - e_c) \left[\frac{1}{2} + \frac{1}{2} \cos\left(4\frac{\pi}{\chi_c}\zeta\right) \right]^n - k \left[\cos\left(\frac{\pi}{\chi_c}\zeta\right) \right]^{10n}, \tag{3}$$

and $\zeta = z/h$ – dimensionless coordinate across the plate thickness, $\chi_c = h_c/h$ – relative thickness of the core, e_c – modulus coefficient, with $0 < e_c \le 1$, n – natural number, k – coefficient ($0 \le k \le 1 - e_c$).

550

Thus, the structure can be classified as a sandwich configuration with an individually tailored functionally graded core. For k=0, it resembles a five-layer structure. It is readily observed that the applied function satisfies the continuity condition of material properties between layers, particularly at $\zeta=-\chi_c/2$, i.e., $f_e(-\chi_c/2)=1$, which results in $E_c(-\chi_c/2)=E_f$. Similarly, the same applies for $\zeta=\chi_c/2$.

Fig. 3 illustrates the post-bending deformation of a straight normal initially perpendicular to the plate's neutral surface.

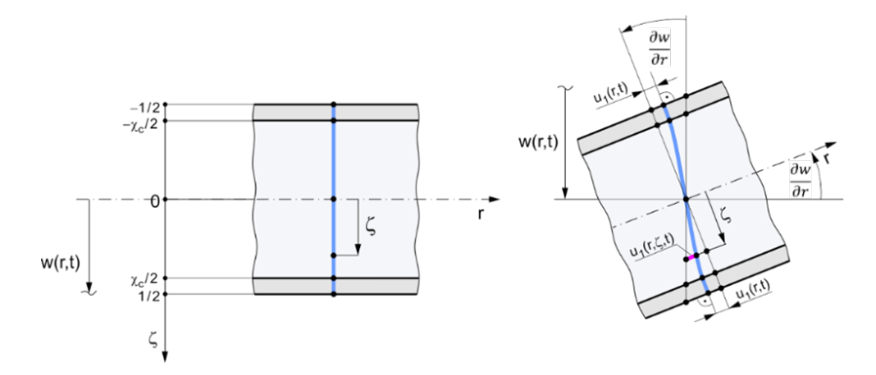


Fig. 3. The deformation scheme of the straight normal line of this plate

The longitudinal displacements, as shown in Fig. 3, are given by:

• the upper facing $(-1/2 \le \zeta \le -\chi_c/2)$

$$u^{(uf)}(r,\zeta,t) = -h \left[\zeta \frac{\partial w}{\partial r} - f_d^{(uf)}(\zeta) \psi(r,t) \right], \tag{4}$$

• the core $(-\chi_c/2 \le \zeta \le \chi_c/2)$

$$u^{(c)}(r,\zeta,t) = -h \left[\zeta \frac{\partial w}{\partial r} - f_d^{(c)}(\zeta) \psi(r,t) \right], \tag{5}$$

• the lower facing $(\chi_c/2 \le \zeta \le 1/2)$

$$u^{(lf)}(r,\zeta,t) = -h \left[\zeta \frac{\partial w}{\partial r} - f_d^{(lf)}(\zeta) \psi(r,t) \right], \tag{6}$$

where: w(r,t) – deflection of the plate, $\psi(r,t) = u_f(r,t)/h$ – dimensionless displacement function, $f_d^{(uf)}(\zeta)$, $f_d^{(c)}(\zeta)$, $f_d^{(lf)}(\zeta)$ – unknown dimensionless deformation functions representing the shape of the deformed straight normal line, t – time.

Therefore, the strains:



• the upper facing $(-1/2 \le \zeta \le -\chi_c/2)$

$$\varepsilon_r^{(uf)}(r,\zeta,t) = \frac{\partial u^{(uf)}}{\partial r} = -h \left[\zeta \frac{\partial^2 w}{\partial r^2} - f_d^{(uf)}(\zeta) \frac{\partial \psi}{\partial r} \right],\tag{7}$$

$$\varepsilon_{\varphi}^{(uf)}(r,\zeta,t) = \frac{u^{(uf)}(r,\zeta,t)}{r} = -h \left[\zeta \frac{\partial w}{r \partial r} - f_d^{(uf)}(\zeta) \frac{\psi(r,t)}{r} \right], \quad (8)$$

$$\gamma_{rz}^{(uf)}(r,\zeta,t) = \frac{\partial u^{(uf)}}{h\partial \zeta} + \frac{\partial w}{\partial r} = \frac{\mathrm{d}f_d^{(uf)}}{\mathrm{d}\zeta}\psi(r,t),\tag{9}$$

• the core $(-\chi_c/2 \le \zeta \le \chi_c/2)$

$$\varepsilon_r^{(c)}(r,\zeta,t) = \frac{\partial u^{(c)}}{\partial r} = -h \left[\zeta \frac{\partial^2 w}{\partial r^2} - f_d^{(c)}(\zeta) \frac{\partial \psi}{\partial r} \right],\tag{10}$$

$$\varepsilon_{\varphi}^{(c)}(r,\zeta,t) = \frac{u^{(c)}(r,\zeta,t)}{r} = -h \left[\zeta \frac{\partial w}{r\partial r} - f_d^{(c)}(\zeta) \frac{\psi(r,t)}{r} \right],\tag{11}$$

$$\gamma_{rz}^{(c)}(r,\zeta,t) = \frac{\partial u^{(c)}}{h\partial \zeta} + \frac{\partial w}{\partial r} = \frac{\mathrm{d}f_d^{(c)}}{\mathrm{d}\zeta}\psi(r,t),\tag{12}$$

• the lower facing $(\chi_c/2 \le \zeta \le 1/2)$

$$\varepsilon_r^{(lf)}(r,\zeta,t) = \frac{\partial u^{(lf)}}{\partial r} = -h \left[\zeta \frac{\partial^2 w}{\partial r^2} - f_d^{(lf)}(\zeta) \frac{\partial \psi}{\partial r} \right],\tag{13}$$

$$\varepsilon_{\varphi}^{(lf)}(r,\zeta,t) = \frac{u^{(lf)}(r,\zeta,t)}{r} = -h \left[\zeta \frac{\partial w}{r\partial r} - f_d^{(lf)}(\zeta) \frac{\psi(r,t)}{r} \right], \quad (14)$$

$$\gamma_{rz}^{(lf)}(r,\zeta,t) = \frac{\partial u^{(lf)}}{h\partial \zeta} + \frac{\partial w}{\partial r} = \frac{\mathrm{d}f_d^{(lf)}}{\mathrm{d}\zeta}\psi(r,t). \tag{15}$$

Consequently, the stresses:

• the upper facing $(-1/2 \le \zeta \le -\chi_c/2)$

$$\sigma_r^{(uf)}(r,\zeta,t) = \frac{E_f}{1-\nu^2} \left[\varepsilon_r^{(uf)}(r,\zeta,t) + \nu \varepsilon_\varphi^{(uf)}(r,\zeta,t) \right], \tag{16}$$

$$\sigma_{\varphi}^{(uf)}(r,\zeta,t) = \frac{E_f}{1-v^2} \left[\varepsilon_{\varphi}^{(uf)}(r,\zeta,t) + v \varepsilon_r^{uf)}(r,\zeta,t) \right], \tag{17}$$

$$\tau_{rz}^{(uf)}(r,\zeta,t) = \frac{E_f}{2(1+\nu)}\gamma_{rz}^{(uf)}(r,\zeta,t),$$
(18)

• the core $(-\chi_c/2 \le \zeta \le \chi_c/2)$

$$\sigma_r^{(c)}(r,\zeta,t) = \frac{E_f}{1-\nu^2} \left[\varepsilon_r^{(c)}(r,\zeta,t) + \nu \varepsilon_{\varphi}^{(c)}(r,\zeta,t) \right] f_e(\zeta), \tag{19}$$

$$\sigma_{\varphi}^{(c)}(r,\zeta,t) = \frac{E_f}{1-\nu^2} \left[\varepsilon_{\varphi}^{(c)}(r,\zeta,t) + \nu \varepsilon_r^{(c)}(r,\zeta,t) \right] f_e(\zeta), \quad (20)$$

$$\tau_{rz}^{(c)}(r,\zeta,t) = \frac{E_f}{2(1+\nu)} \gamma_{rz}^{(c)}(r,\zeta,t) f_e(\zeta), \tag{21}$$

• the lower facing $(\chi_c/2 \le \zeta \le 1/2)$

$$\sigma_r^{(lf)}(r,\zeta,t) = \frac{E_f}{1-\nu^2} \left[\varepsilon_r^{(lf)}(r,\zeta,t) + \nu \varepsilon_{\varphi}^{(lf)}(r,\zeta,t) \right], \tag{22}$$

$$\sigma_{\varphi}^{(lf)}(r,\zeta,t) = \frac{E_f}{1-\nu^2} \left[\varepsilon_{\varphi}^{(lf)}(r,\zeta,t) + \nu \varepsilon_r^{(lf)}(r,\zeta,t) \right], \tag{23}$$

$$\tau_{rz}^{(lf)}(r,\zeta,t) = \frac{E_f}{2(1+\nu)} \gamma_{rz}^{(lf)}(r,\zeta,t),$$
(24)

where ν – Poisson's ratio, assumed to be constant throughout the entire plate.

The unknown dimensionless deformation functions of the straight normal line $f_d^{(uf)}(\zeta)$, $f_d^{(c)}(\zeta)$, $f_d^{(lf)}(\zeta)$ (Fig. 3) are consistent with those presented in paper [19]. Moreover, procedures for their derivation are described in detail in papers [16] and [20], with consideration of the Zhuravsky (Jourawski) shear stress. Thus, these functions are in following forms:

• the upper facing $(-1/2 \le \zeta \le -\chi_c/2)$

$$f_d^{(uf)}(\zeta) = C_f + \frac{1}{24} \left(3 - 4\zeta^2 \right) \zeta,$$
 (25)

• the core $(-\chi_c/2 \le \zeta \le \chi_c/2)$

$$f_d^{(c)}(\zeta) = \int \frac{\bar{S}_z^{(c)}(\zeta)}{f_e(\zeta)} d\zeta, \qquad (26)$$

• the lower facing $(\chi_c/2 \le \zeta \le 1/2)$

$$f_d^{(lf)}(\zeta) = -C_f + \frac{1}{24} \left(3 - 4\zeta^2 \right) \zeta,$$
 (27)

where

$$\begin{split} \bar{S}_{z}^{(c)}(\zeta) &= \frac{1}{8} \left[1 - \chi_{c}^{2} + e_{c} \left(\chi_{c}^{2} - 4 \zeta^{2} \right) \right] - (1 - e_{c}) J_{c1}(\zeta) + k J_{c2}(\zeta), \\ J_{c1}(\zeta) &= \int_{-\chi_{c}/2}^{\zeta} \left[\frac{1}{2} + \frac{1}{2} \cos \left(4 \frac{\pi}{\chi_{c}} \zeta_{1} \right) \right]^{n} \zeta_{1} d\zeta_{1}, \\ J_{c2}(\zeta) &= \int_{-\chi_{c}/2}^{\zeta} \left[\cos \left(\frac{\pi}{\chi_{c}} \zeta_{1} \right) \right]^{10n} \zeta_{1} d\zeta_{1}, \end{split}$$



$$C_f = \frac{1}{48} \left(3 - \chi_c^2 \right) \chi_c - \int_0^{\chi_c/2} \frac{\bar{S}_z^{(c)}(\zeta)}{f_e(\zeta)} \, d\zeta.$$

Functions (25) and (27) corresponding to the upper and lower facings satisfy the necessary condition, i.e., they are perpendicular to the external surfaces of this plate.

Fig. 4 presents the variation of Young's modulus as described by equation (3), along with the deformation profile of the straight normal line based on expressions (25), (26), and (27), for the representative plate configuration defined by $\chi_c = 22/25$, $e_c = 1/25$, n = 5, k = 0.5.

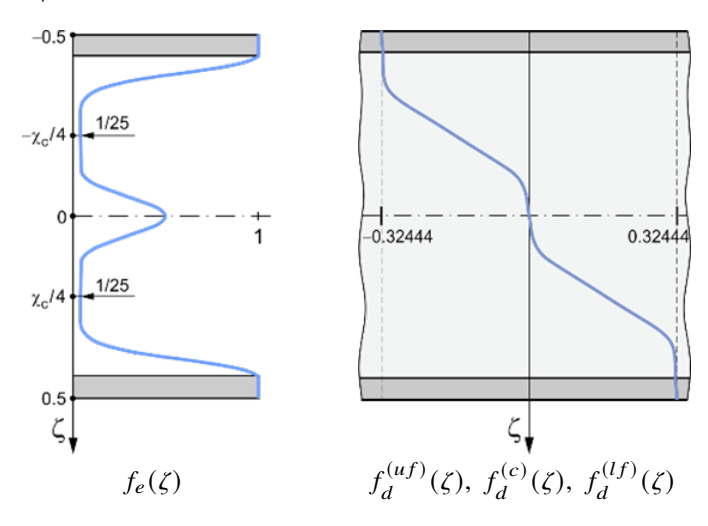


Fig. 4. Variation of Young's modulus and deformation of the initially straight normal line

3. The analytical study of the free flexural axisymmetric vibration of the plate

The kinetic energy of the plate is expressed as:

$$U_k = \pi \rho_p h \int_0^R \left(\frac{\partial w}{\partial t}\right)^2 r \, \mathrm{d}r,\tag{28}$$

where the mass density of the plate

$$\rho_p = \rho_f \left[1 - \chi_c + \int_{-\chi_c/2}^{\chi_c/2} f_\rho(\zeta) \,\mathrm{d}\zeta \right],\tag{29a}$$

the dimensionless function, in accordance with the article [18], is as follows

$$f_{\rho}(\eta) = \sqrt{e_c} + \left(1 - \sqrt{e_c}\right) \left[\frac{1}{2} + \frac{1}{2}\cos\left(4\frac{\pi}{\chi_c}\zeta\right)\right]^n - k\left[\cos\left(\frac{\pi}{\chi_c}\zeta\right)\right]^{10n}, \quad (29b)$$

Ewa MAGNUCKA-BLANDZI, Krzysztof MAGNUCKI

and ρ_f is mass density of the facing material.

The elastic strain energy

$$U_{\varepsilon,\gamma} = \pi \frac{E_f h}{1 - v^2} \int_0^R \left[\Phi_{\varepsilon,\gamma}^{(uf)}(r,t) + \Phi_{\varepsilon,\gamma}^{(c)}(r,t) + \Phi_{\varepsilon,\gamma}^{(lf)}(r,t) \right] r \, \mathrm{d}r, \tag{30}$$

where:

$$\begin{split} \Phi_{\varepsilon,\gamma}^{(uf)}(r,t) &= \int\limits_{-1/2}^{-\chi_c/2} \left\{ \left[\varepsilon_r^{(uf)}(r,\zeta,t) \right]^2 + 2\nu \varepsilon_r^{(uf)}(r,\zeta,t) \varepsilon_\varphi^{(uf)}(r,\zeta,t) \right. \\ &+ \left[\varepsilon_\varphi^{(uf)}(r,\zeta,t) \right]^2 + \frac{1-\nu}{2} \left[\gamma_{rz}^{(uf)}(r,\zeta,t) \right]^2 \right\} r \, \mathrm{d}r, \\ \Phi_{\varepsilon,\gamma}^{(c)}(r,t) &= \int\limits_{-\chi_c/2}^{-\chi_c/2} \left\{ \left[\varepsilon_r^{(c)}(r,\zeta,t) \right]^2 + 2\nu \varepsilon_r^{(c)}(r,\zeta,t) \varepsilon_\varphi^{(c)}(r,\zeta,t) \right. \\ &+ \left[\varepsilon_\varphi^{(c)}(r,\zeta,t) \right]^2 + \frac{1-\nu}{2} \left[\gamma_{rz}^{(c)}(r,\zeta,t) \right]^2 \right\} r \, \mathrm{d}r, \\ \Phi_{\varepsilon,\gamma}^{(lf)}(r,t) &= \int\limits_{\chi_c/2}^{1/2} \left\{ \left[\varepsilon_r^{(lf)}(r,\zeta,t) \right]^2 + 2\nu \varepsilon_r^{(lf)}(r,\zeta,t) \varepsilon_\varphi^{(lf)}(r,\zeta,t) \right. \\ &+ \left[\varepsilon_\varphi^{(lf)}(r,\zeta,t) \right]^2 + \frac{1-\nu}{2} \left[\gamma_{rz}^{(lf)}(r,\zeta,t) \right]^2 \right\} r \, \mathrm{d}r. \end{split}$$

Based on Hamilton's principle $\delta \int_{t_1}^{t_2} (U_k - U_{\varepsilon,\gamma}) dt = 0$, and considering the ex-

pressions for kinetic energy (28) and elastic strain energy (30), two differential equations of motion for the clamped circular plate are obtained in the following form:

$$\rho_{p}hr\frac{\partial^{2}w}{\partial t^{2}} + D_{o}\frac{\partial}{\partial r}\left\{r\frac{\partial}{\partial r}\left[\frac{1}{r}\frac{\partial}{\partial r}\left(r\left(C_{ww}\frac{\partial w}{\partial r} - C_{w\psi}\psi(r,t)\right)\right)\right]\right\} = 0, \quad (31)$$

$$\frac{\partial}{\partial r}\left\{\frac{1}{r}\frac{\partial}{\partial r}\left[r\left(C_{w\psi}\frac{\partial w}{\partial r} - C_{\psi\psi}\psi(r,t)\right)\right]\right\} + C_{\psi}\frac{\psi(r,t)}{h^{2}} = 0, \quad (32)$$



where dimensionless coefficients:

$$\begin{split} C_{ww} &= 1 - \chi_c^3 + 12 \int_{-\chi_c/2}^{\chi_c/2} \zeta^2 f_e(\zeta) \, \mathrm{d}\zeta, \\ C_{\psi\psi} &= 12 \left\{ 2 \int_{\chi_c/2}^{1/2} \left[f_d^{(lf)}(\zeta) \right]^2 \, \mathrm{d}\zeta + \int_{-\chi_c/2}^{\chi_c/2} \left[f_d^{(c)}(\zeta) \right]^2 f_e(\zeta) \, \mathrm{d}\zeta \right\}, \\ C_{w\psi} &= -3 \left(1 - \chi_c^2 \right) C_f + \frac{1}{40} \left(4 - 5\chi_c^3 + \chi_c^5 \right) + 12 \int_{-\chi_c/2}^{\chi_c/2} \zeta f_d^{(c)}(\zeta) f_e(\zeta) \, \mathrm{d}\zeta, \\ C_{\psi} &= \frac{1 - \nu}{2} \left[\frac{1}{80} \left(8 - 15\chi_c + 10\chi_c^3 - 3\chi_c^5 \right) \right] + 12 \int_{-\chi_c/2}^{\chi_c/2} \frac{\left[\bar{S}_z^{(c)}(\zeta) \right]^2}{f_e(\zeta)} \, \mathrm{d}\zeta, \end{split}$$

and

$$D_o = \frac{E_f h^3}{12(1 - v^2)}$$
 [Nmm].

The two differential equations of motion, (31) and (32), are approximately solved by assuming the following forms for the functions:

$$w(r,t) = \left[1 - \left(\frac{r}{R}\right)^2\right]^2 w_a(t), \qquad \psi(r,t) = \left[1 - \left(\frac{r}{R}\right)^2\right] \frac{r}{R} \psi_a(t), \tag{33}$$

where $w_a(t)$, $\psi_a(t)$ – functions of the time.

These assumed functions satisfy the boundary conditions of the clamped plate: w(R,t) = 0, $\partial w/\partial r\big|_0 = 0$, $\partial w/\partial r\big|_R = 0$, $\psi(0,t) = \psi(R,t) = 0$. Substituting these functions into the motion equations (31) and (32), and applying Galerkin's method, after simple transformations, one obtains:

$$\psi_a(t) = \frac{56C_{w\psi}}{14C_{\psi\psi} + C_{\psi} (R/h)^2} \frac{w_a(t)}{R},$$
(34)

and the differential equation

$$\frac{\mathrm{d}^2 w_a}{\mathrm{d}t^2} + \frac{320}{3} \left(1 + C_{se} \right) C_{ww} \frac{D_o}{\rho_p h R^4} w_a(t) = 0, \tag{35}$$

where dimensionless coefficient of the shear effect

$$C_{se} = \frac{14C_{w\psi}^2}{14C_{\psi\psi} + C_{\psi} (R/h)^2} \frac{1}{C_{ww}}.$$
 (36)

Ewa MAGNUCKA-BLANDZI, Krzysztof MAGNUCKI

Equation (35) is solved by assuming the following form of the solution:

$$w_a(t) = w_a \sin(\omega t), \tag{37}$$

where: w_a – amplitude of the flexural vibration, ω – fundamental natural frequency. Substituting the assumed solution (37) into the differential equation (35), one obtains the fundamental natural frequency as follows

$$\omega = \frac{8 \cdot 10^6}{R^2} \sqrt{\frac{5}{3} (1 + C_{se}) \frac{D_p}{\rho_p h}}$$
 [1/s], (38a)

or

$$\frac{\omega}{2\pi} = \frac{4 \cdot 10^6}{\pi R^2} \sqrt{\frac{5}{3} (1 + C_{se}) \frac{D_p}{\rho_p h}}$$
 [Hz], (38b)

where: the flexural rigidity of the plate $D_p = C_{ww}C_o$ [Nmm] and h [mm], R [mm], E_f [MPa], ρ_p [kg/m³].

Moreover, the mass of the plate

$$m_p = \pi \frac{R^2 h}{10^9} \rho_p \text{ [kg]}.$$
 (39)

Exemplary calculations are conducted for two circular sandwich plates, both having the same total thickness but differing core thicknesses. The material and geometric data for both plates are as follows: $E_f = 72000$ MPa, $\rho_f = 2710$ kg/m³, Young's modulus coefficient $e_c = 1/25$, Poisson's ratio $\nu = 0.3$, radius R = 400 mm, total thickness h = 25 mm, material exponent n = 5, 20, and coefficient k = 0, 0.25, 0.50, 0.75, 0.96.

• First plate specifications: core thickness $h_c = 22$ mm, facing thickness $h_f = 1.5$ mm, thus $\chi_c = 22/25$.

The computational outcomes are presented in Tables 1 and 2, with corresponding graphical results illustrated in Figs. 5 and 6.

Table 1. First plate – Selected results of exemplary calculations for material exponent n = 5

k	0	0.25	0.50	0.75	0.96
C_{ww}	0.554492	0.554036	0.553580	0.553124	0.552741
C_{se}	0.0988801	0.100362	0.102386	0.105914	0.117268
$\omega/2\pi$ [Hz]	456.50	469.14	482.97	498.44	514.51
m_p [kg]	15.98025	15.13907	14.29790	13.45673	12.75014



Table 2. First p	late – Selected	results of exem	plary calculation	ns for materia	l exponent $n = 20$

k	0	0.25	0.50	0.75	0.96
C_{ww}	0.459644	0.459587	0.459528	0.459471	0.459422
C_{se}	0.108055	0.108566	0.109286	0.110563	0.114864
$\omega/2\pi$ [Hz]	461.22	468.92	477.06	485.75	494.14
m_p [kg]	13.08596	12.66379	12.24162	11.81946	11.46484

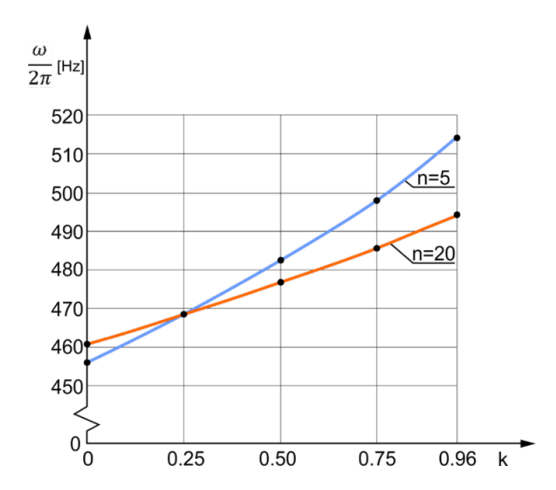


Fig. 5. Fundamental natural frequency of the first plate configuration

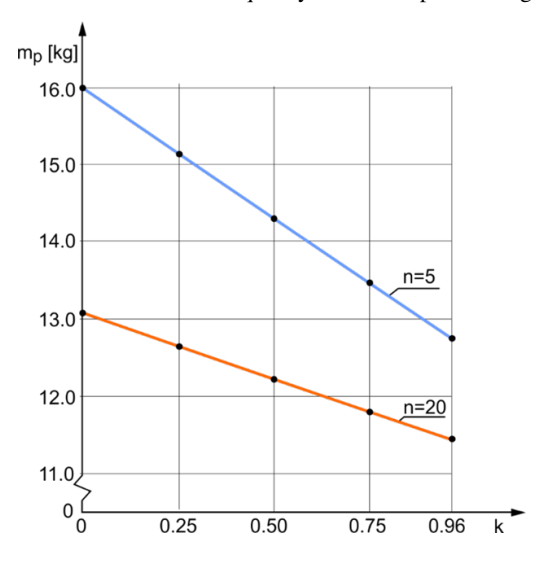


Fig. 6. Mass of the first plate configuration

• Second plate specifications: core thickness $h_c=20$ mm, facing thickness $h_f=2.5$ mm, thus $\chi_c=20/25$.

558

The computational results for the second sandwich plate configuration are detailed in Tables 3 and 4, with their graphical counterparts illustrated in Figs. 7 and 8.

k	0	0.25	0.50	0.75	0.96
C_{ww}	0.665283	0.664941	0.664598	0.664255	0.663968
C_{se}	0.114099	0.115710	0.117944	0.121836	0.134382
$\omega/2\pi$ [Hz]	479.44	490.42	502.31	515.45	529.42
m_n [kg]	17.62339	16.85869	16.09399	15.32928	14.68693

Table 3. Second plate – Selected results of exemplary calculations for material exponent n = 5

Table 4. Second plate – Selected results of exemplary calculations for material exponent n = 20

k	0	0.25	0.50	0.75	0.96
C_{ww}	0.594023	0.593979	0.593936	0.593892	0.593856
C_{Se}	0.133176	0.133772	0.134601	0.136077	0.141105
$\omega/2\pi$ [Hz]	495.37	501.95	508.84	516.17	523.42
m_p [kg]	14.99222	14.60843	14.22464	13.84086	13.51847

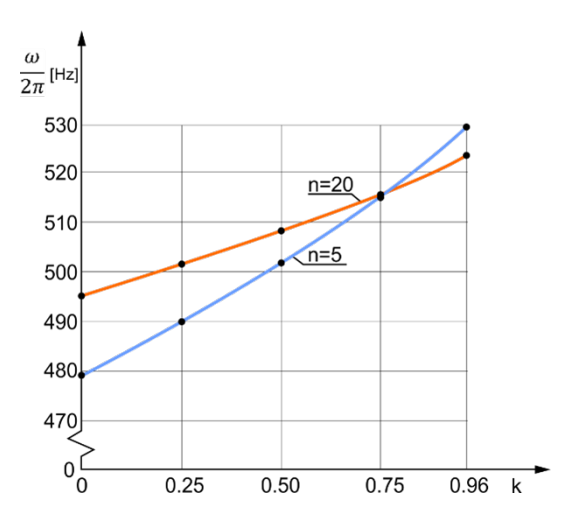


Fig. 7. Fundamental natural frequency of the second plate configuration

The variability in the core structure – reflected in the mechanical properties described by Eq. (2) and the core thickness ratio – has a pronounced influence on both the fundamental natural frequency and the mass of the plate. It is governed by the material exponent n and the coefficient k ($0 \le k \le 1 - e_c$), both of which are incorporated into the dimensionless displacement function $f_e(\zeta)$ defined in expression (3).

However, in the particular case of a homogeneous plate – a single-layer structure characterized by $e_c = 1$ and k = 0 – the graphs of the Young's modulus

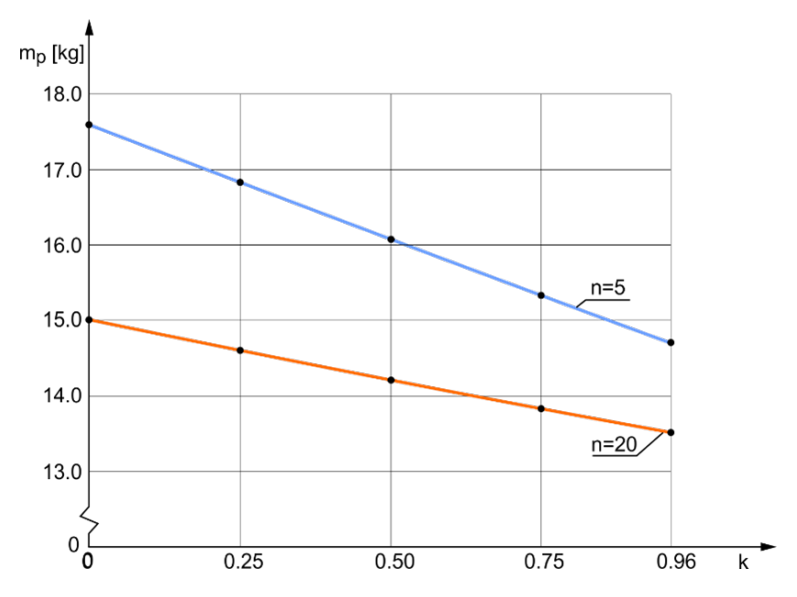


Fig. 8. Mass of the second plate configuration

variation (3) and the deformation of the straight normal line (25), (26), and (27) are presented in Fig. 9.

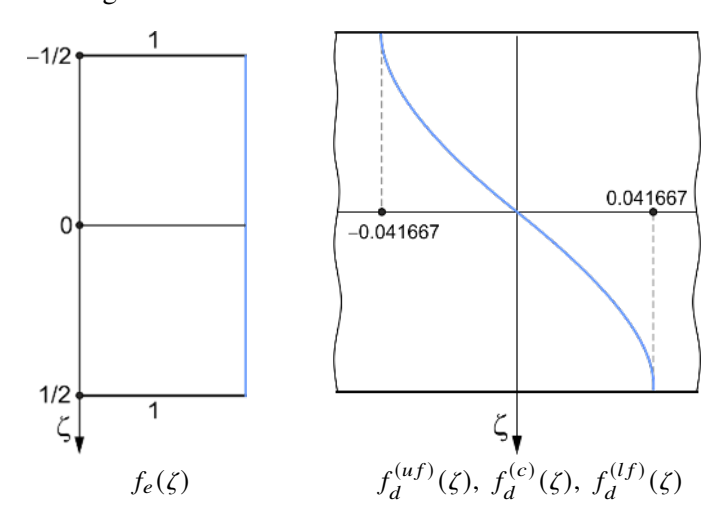


Fig. 9. Young's modulus and deformation of the initially straight normal line

Moreover, the values of the dimensionless coefficients appearing in equations (31) and (32) are as follows: $C_{ww} = 1$, $C_{w\psi} = 0.1$, $C_{\psi\psi} = 0.010119$, $C_{\psi} = 0.035$. Therefore, the dimensionless shear effect coefficient (36) is $C_{se} = 0.0153818$. It can be readily observed that these values are independent of the material exponent n-10 a natural number. Consequently, the values of the fundamental natural frequencies (38b) for this plate are as follows:

- with the shear effect $\frac{\omega}{2\pi}$ = 403.682 Hz,
- without the shear effect ($C_{se} = 0$) the classical solution $\frac{\omega}{2\pi} = 400.613$ Hz.

4. Conclusions

These dimensionless deformation functions $f_d^{(uf)}(\zeta)$ (25), $f_d^{(c)}(\zeta)$ (26), $f_d^{(lf)}(\zeta)$ (27) of the straight normal line, adopted from article [19], enhance the analytical model of the circular plate. These functions are derived with consideration of the classical shear stress formula, known as Zhuravsky (Jourawski) shear stress.

The proposed variation of Young's modulus (expression (2)) across the core thickness of the plate – formulated as a single continuous function – enables an analytical description of a sandwich structure composed of two facings with constant mechanical properties and a core with variable properties. This unified model can represent a homogeneous single-layer, a three-layer configuration (with a nearly constant-property core), a five-layer-like structure, and all intermediate configurations, within a single analytical framework. Thus:

- homogeneous one-layer structures for $e_c = 1$ and k = 0,
- similar to three-layer structures for $k = 1 e_c$,
- similar to five-layer structures for k = 0.

The variability of the core structure and the core thickness ratio have a significant impact on both the fundamental natural frequency and the mass of the plate.

References

- [1] N.E. Meiche, A. Tounsi, N. Ziane, I. Mechab, and E.A. Adda Bedia. A new hyperbolic shear deformation theory for buckling and vibration of functionally graded sandwich plate. *International Journal of Mechanical Sciences*, 53(4):237–247, 2011. doi: 10.1016/j.ijmecsci.2011.01.004.
- [2] H-T. Thai and T.P. Vo. A new sinusoidal shear deformation theory for bending, buckling, and vibration of functionally graded plates. *Applied Mathematical Modelling*, 37(5):3269–3281, 2013. doi: 10.1016/j.apm.2012.08.008.
- [3] A. Mahi, E.A. Adda Bedia, and A. Tounsi. A new hyperbolic shear deformation theory for bending and free vibration analysis of isotropic, functionally graded, sandwich and laminated composite plates. *Applied Mathematical Modelling*, 39(9):2489–2508, 2015. doi: 10.1016/j.apm.2014.10.045.
- [4] D. Chen, J. Yang, and S. Kitipornchai. Free and forced vibrations of shear deformable functionally graded porous beams. *International Journal of Mechanical Sciences*, 108-109:14–22, 2016. doi: 10.1016/j.ijmecsci.2016.01.025.
- [5] D.B. Singh and B.N. Singh. New higher order shear deformation theories for free vibration and buckling analysis of laminated and braided composite plates. *International Journal of Mechanical Sciences*, 131-132:265–277, 2017. doi: 10.1016/j.ijmecsci.2017.06.053.

- [6] Y. Zhai, Y. Li, and S. Liang. Free vibration analysis of five-layered composite sandwich plates with two-layered viscoelastic cores. Composite Structures, 200:346-357, 2018. doi: 10.1016/j.compstruct.2018.05.082.
- [7] K.K. Zur. Quasi-Green's function approach to free vibration analysis of elastically supported functionally graded circular plates. Composite Structures, 183:600-610, 2018. doi: 10.1016/j.compstruct.2017.07.012.
- [8] V. Birman and G.A. Kardomateas. Review of current trends in research and applications of sandwich structures. Composites Part B: Engineering, 142:221-240, 2018. doi: 10.1016/j.compositesb.2018.01.027.
- [9] K. Magnucki, D. Witkowski, and E. Magnucka-Blandzi. Buckling and free vibrations of rectangular plates with symmetrically varying mechanical properties – Analytical and FEM studies. Composite Structures, 220:355–361, 2019. doi: 10.1016/j.compstruct.2019.03.082.
- [10] K.K. Zur, M. Arefi, J. Kim, and J.N. Reddy. Free vibration and buckling analyses of magneto-electro-elastic FGM nanoplates based on nonlocal modified higher-order sinusoidal shear deformation theory. Composites Part B: Engineering, 182:107601, 2020. doi: 10.1016/j.compositesb.2019.107601.
- [11] M.Z. Roshanbakhsh, S.M. Tavakkoli, and B. Navayi Neya. Free vibration of functionally graded thick circular plates: An exact and three-dimensional solution. International Journal of Mechanical Sciences, 188:105967, 2020. doi: 10.1016/j.ijmecsci.2020.105967.
- [12] K. Magnucki K. Free axisymmetric flexural vibrations of circular plate with symmetrically varying mechanical properties supported on elastic foundation. Vibrations in Physical Systems, 31(2):2020217, 2020. doi: 10.21008/j.0860-6897.2020.2.17.
- [13] E. Magnucka-Blandzi, K. Magnucki, and W. Stawecki. Bending and buckling of a circular plate with symmetrically varying mechanical properties. Applied Mathematical Modelling, 89(2):1198–1205, 2021. doi: 10.1016/j.apm.2020.07.031.
- [14] S.K. Sah and A. Ghosh. Influence of porosity distribution on free vibration and buckling analysis of multi-directional functionally graded sandwich plates. Composite Structures, 279:114795, 2022. doi: 10.1016/j.compstruct.2021.114795.
- [15] L. Wei and H. Qing. Bending, buckling and vibration analysis of Bi-directional functionally graded Circular/Annular microplate based on MCST. Composite Structures, 292:115633, 2022. doi: 10.1016/j.compstruct.2022.115633.
- [16] K. Magnucki. An individual shear deformation theory of beams with consideration of the Zhuravsky shear stress formula. In: A. Zingoni (ed.) Current Perspectives and New Directions in Mechanics, Modelling and Design of Structural Systems, pages 682–689, CRC Press, 2022, doi: 10.1201/9781003348443-112.
- [17] K. Magnucki and E. Magnucka-Blandzi. Free flexural axisymmetric vibrations of generalized circular sandwich plate. In: Z. Dimitrová, P. Biswas, R. Gonçalves, T. Silva (eds.) Recent Trends in Wave Mechanics and Vibrations, Proceedings of WMVC 2022, pages 219-229, Springer, 2023. doi: 10.1007/978-3-031-15758-5_21.
- [18] K. Magnucki, E. Magnucka-Blandzi, and K. Sowiński. Buckling and free flexural vibration of an asymmetric sandwich beam with a functionally graded core. Archives of Mechanics, 76(4):335–355, 2024. doi: 10.24423/aom.4532.
- [19] K. Magnucki, E. Magnucka-Blandzi, and K. Sowiński. Elastic buckling of a rectangular sandwich plate with individual functionally graded core. Journal of Theoretical and Applied Mechanics, 62(1):171-185, 2024. doi: 10.15632/jtam-pl/178521.
- [20] L. Bardella. Explicit analytical solutions for the full plane-stress field in sandwich beams under flexure governed by zigzag warping. Composite Structures, 329:117754, 2024. doi: 10.1016/j.compstruct.2023.117754.